The nature of surface defects in Xe ion-implanted glassy carbon annealed at high temperatures: Raman spectroscopy analysis

M.J. Madito[a],*, M.Y.A. Ismail[b], T.T. Hlatshwayo[b] and C.B. Mtshali[a]

[a] iThemba LABS, National Research Foundation, PO Box 722, Somerset West 7129, Cape Town, South Africa
[b] Department of Physics, University of Pretoria, Private Bag X20, Pretoria 0002, South Africa

∗Corresponding author. E-mail address: mmadito@tlabs.ac.za (M.J. Madito).

Highlights

- Polished glassy carbon (GC) were implanted with 200 keV Xe ions.
- Xe implanted glassy carbon (Xe-GC) samples were annealed at 500, 1000 and 1500 °C under vacuum.
- During polishing of the GC, the crystallites size reduced and sp^3-type of defects were introduced.
- The sp^3-type of defects were modified by ion implantation to boundary-like defects in graphite.
- The boundary-like defects did not change during annealing.

Abstract

The mechanically polished glassy carbon (GC) samples were implanted with 200 keV Xe ions to a fluence of 1×10^{16} cm^{-2} at room temperature. The Monte Carlo simulation code, Stopping and Range of Ions in Matter (SRIM) was used to simulate the Xe ions implanted in GC. At the surface of the implanted GC, a dose of 6.53 displacements per atom which corresponds to the nuclear energy loss of 0.142 keV/nm (SRIM prediction) amorphized the GC structure. Raman spectroscopy, a well-established tool to probe disorder in carbonaceous materials through Raman-based disorder signature (D-band) relative to the Raman-allowed first-order band (G-band), confirmed that ion bombardment resulted in GC amorphization. And also showed that during mechanical polishing of the GC the sp^3-type of defects were introduced which describe the out-of-plane atoms bonded to carbon atoms. This sp^3-type of defects was modified by ion implantation to boundary-like defects in graphite. The Xe implanted GC (Xe-GC) samples were annealed from 100 up to 500, 1000 and 1500 °C in steps of 100 °C for 5 h per step under vacuum. Recovery of the amorphized structure of the Xe-GC samples was not observed at temperatures ≤1000 °C, however, at 1500 °C about 54% of the structure was recovered.

Keywords: Glassy carbon; Sp^3 hybridization; Boundary defects; Xe ions; Ion implantation; Raman spectroscopy

1. Introduction

One of the emphases on the management of nuclear waste (i.e. fission products) is long-term isolation or storage. Consequently, research focus has been on the long-term performance of radiation-resistant materials as barriers to nuclide migration or release [1]. There has been an interest in employing the disordered, non-graphitizing glassy carbon (GC) as a barrier to radioactive fission products due to its diverse range of physical properties, such as high thermal resistance, extreme chemical stability, low density and great hardness, and gases impermeability [2]. GC combines glassy and ceramic properties, and is commercially manufactured by controlled degradation of certain polymers at temperatures in the range of 900–1000 °C and can be easily polished. GC is also a class of non-graphitizing carbon that is extensively used as a counter electrode in electrochemistry and has been used for ion implantation [3], [4], [5], [6], [7].

Commercial glassy carbons contain a high proportion of fullerene-like structures consisting of broken and imperfect fullerene fragments in the form of curved sp^2-bonded graphene-like planes which often surround closed pores [8], [9], [10], [11]. Such curvature has been attributed to the surface topological defects [8], [9]. Jurkiewicz et al. have demonstrated that the fullerene-like structure of glassy carbons is responsible for their high hardness and strength [2]. Typically, the GC structure is a key factor determining porosity, mechanical, and electronic properties. In carbon-related materials, structural and mechanical properties can be improved/modified by introducing controlled amounts of lattice defects [2]. The ion implantation technique has been widely used to introduce foreign species into a target material and to alter the level of disorder within the target leading to desirable changes in the surface properties of materials. On the other hand, Raman spectroscopy which is less destructive and provides structural information and transformation between the crystalline and amorphous state of the material, has been largely used to probe disorder in the sp^2-network of different carbon structures through defect-activated vibration modes [12], [13], [14], [15], including the nature of disorder/defects, particularly in graphene [16]. In the characterisation of ion-implanted GC samples, Raman spectroscopy has been used to demonstrate the transformation between the crystallinity and amorphisation upon ion implantation [4], [5], [17], [18].

Despite previously published reports on the surface structure (or structural and mechanical properties) of GC and ion-implanted GC, the reports on the nature of surface defects in ion implanted GC are lacking in the literature. The defects, in general, can be defined as grain boundaries, vacancies, (self-) interstitials, implanted atoms, and sp^3-type of defects associated with a change of carbon-hybridisation (sp^2-to-sp^3) [16]. The nature of surface defects strongly depends on the treatment of the sample. For instance, irradiation or ion implantation causes atoms to be displaced from their lattice sites to form defects by nuclear collisions. This study aims at reporting the nature of surface defects in Xe ion-implanted GC (Xe-GC) samples annealed at high temperatures. Heavy ions are ideal for ion-beam-induced damage studies of GC since they create a large damage density in the carbon matrix at doses in the order of $\sim 10^{16}$ cm^{-2} [7].

2. Experimental

Commercial GC (Sigradur® G) samples were mechanically polished to a mirror finish with 1 and 0.5 µm diamond solutions, and thereafter, the samples were cleaned consecutively in an ultrasonic bath with alkaline soap, de-ionized water, methanol and dried with nitrogen gas.

The polished GC samples were implanted at the perpendicular incidence beam direction and room temperature by 200 keV Xe ions to a fluence of 1×10^{16} cm^{-2}. During the implantation, the beam was raster scanned. Some of the Xe-GC samples were annealed from 100 up to 500, 1000 and 1500 °C in steps of 100 °C for 5 h per step under vacuum. Therefore, a total annealing time for a sample annealed up to 500, 1000 and 1500 °C was 25, 50 and 75 h, respectively. During annealing, the base pressure of the vacuum was $\sim 10^{-7}$ mbar attained by Pfeiffer Vacuum magnetically levitated turbopump with a pumping speed of 255 l/s for N_2. SRIM (2013 version) was used to simulate the Xe ions in GC and an option ''Detailed Calculation with full Damage Cascades'' was used to compute the ion-induced displacement damage parameters. The calculations were carried out using 10 000 incident ions and the threshold displacement energy of 25 eV for C [19]. The lattice binding energy was set to zero [20]. Moreover, WITec alpha300 confocal Raman microscope was used for analyses that were carried out using a 100×/0.9NA objective and 532 nm laser at a power of 5 mW. The Raman image scans were acquired over a 40 μm^2 area with 200 points per line and 200 lines per image (40 000 spectra per image) using an integration time of 0.1 s. The average Raman spectra were acquired using an integration time of 30 s and 10 accumulations, and the signal was stable during measurements. For 100×/0.9NA objective the diffraction-limited lateral resolution is about 361 nm. The spectral resolution is in the order of 1 cm^{-1}.

3. Results and discussion

Fig. 1 displays SRIM simulation results of 200 keV Xe ions implanted into GC at the perpendicular incidence and room temperature. Fig. 1(a) shows trajectories of Xe ions in GC which have nearly Gaussian profile with a projected mean range $R_p = 120.6$ nm and straggling of $\Delta R_p = 21.6$ nm (Fig. 1(b)). Fig. 1(c) shows the subcascades generated by recoiling lattice atoms distributed along the Xe ions trajectories. To compare damage produced by different ions in solid target materials it is often convenient to calculate displacements per atom (dpa) for a given ion dose. The number of GC-atom vacancies per ion per nanometer produced by Xe ions were converted into dpa (Fig. 1(d)) as follows:

$$dpa = \frac{(Vacancies/ion \cdot nm) \times 10^7}{N_a} \times \varphi \quad (1)$$

where φ (ions/cm^2) is the ion fluence, N_a is the atomic density ($N_a = 7.119 \times 10^{22}$ atoms/cm^3 for Sigradur® GC), and 10^7 is the conversion factor from nanometer to a centimetre.

As 200 keV Xe ions impinge GC, they lose energy via electronic and nuclear collision processes (Fig. 1(e)) until they come to rest. The latter process is responsible for radiation-damage effects (i.e. dpa). The electronic and nuclear energy loss values at the surface of the GC are 0.478 and 0.142 keV/nm, respectively. The nuclear energy loss of 0.142 keV/nm corresponds to 6.53 dpa at the surface of the GC. In the implanted layer, the maximum nuclear energy loss is 0.817 keV/nm which corresponds to 23.0 dpa. These values are much higher than the minimum value (0.2 dpa) where the graphitic bonding within the GC structure begins to break up (i.e. the production of approximately one vacancy per lattice carbon in the graphitic ribbons which make up GC) [7]. McCulloch et al. showed that a 320 keV Xe ions at a dose of 5×10^{15} cm^{-2} which corresponds to 4 dpa at the surface, completely amorphized the GC structure [7]. In our work, the Raman spectrum of the implanted surface layer (Fig. 2) is very similar to that obtained from amorphous carbons, which suggests that the ion implantation (6.53 dpa) has amorphized the surface layer of the GC.

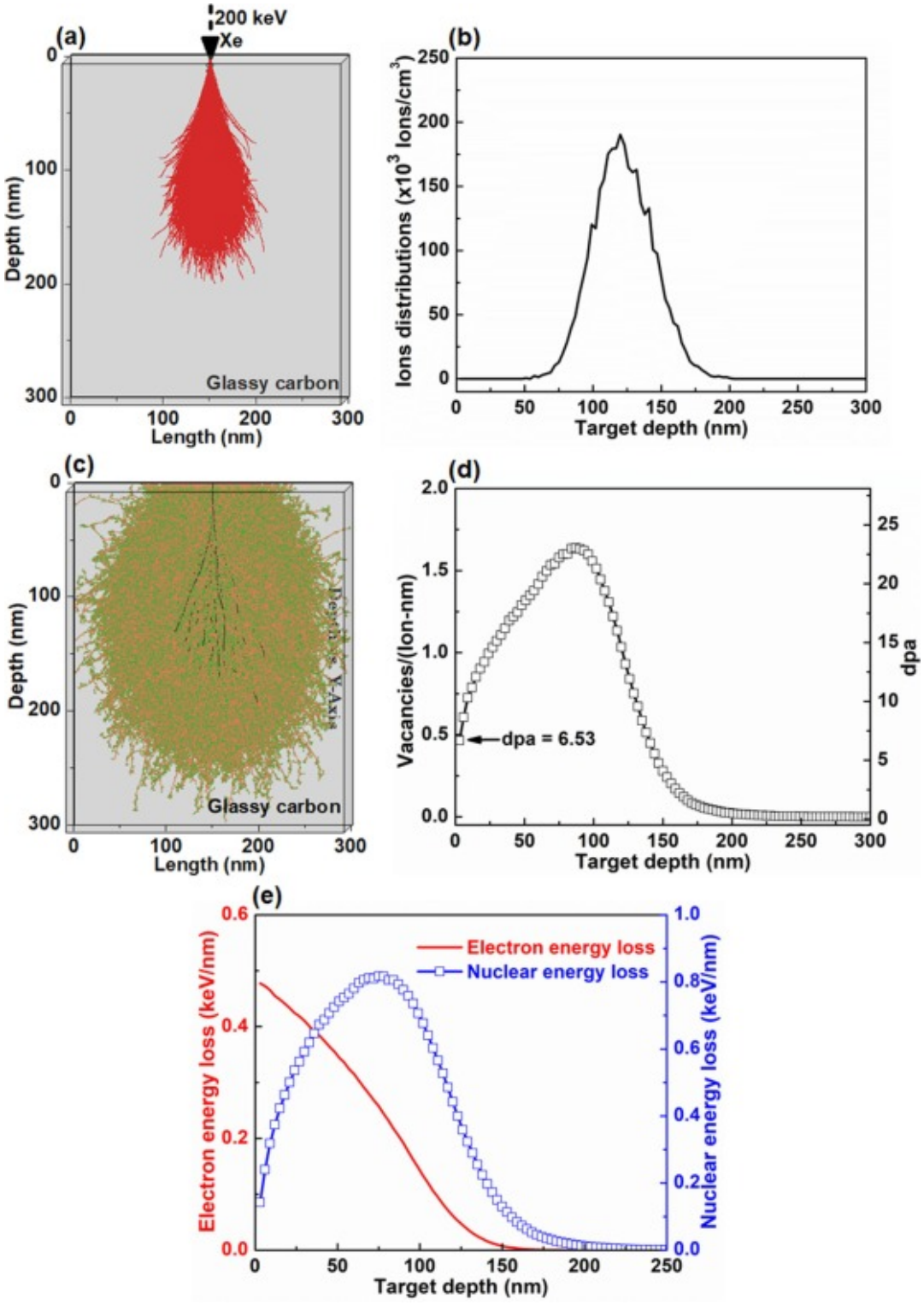

Fig. 1. SRIM calculations of 200 keV Xe ions in GC: (a) Trajectories of Xe ions in GC. (b) Ion distributions profile. (c) The subcascades generated by recoiling lattice atoms distributed along the Xe ions trajectories. (d) GC-atom vacancies per ion per nanometer and the corresponding displacements per atom (dpa). (e) The electron and nuclear energy loss with depth.

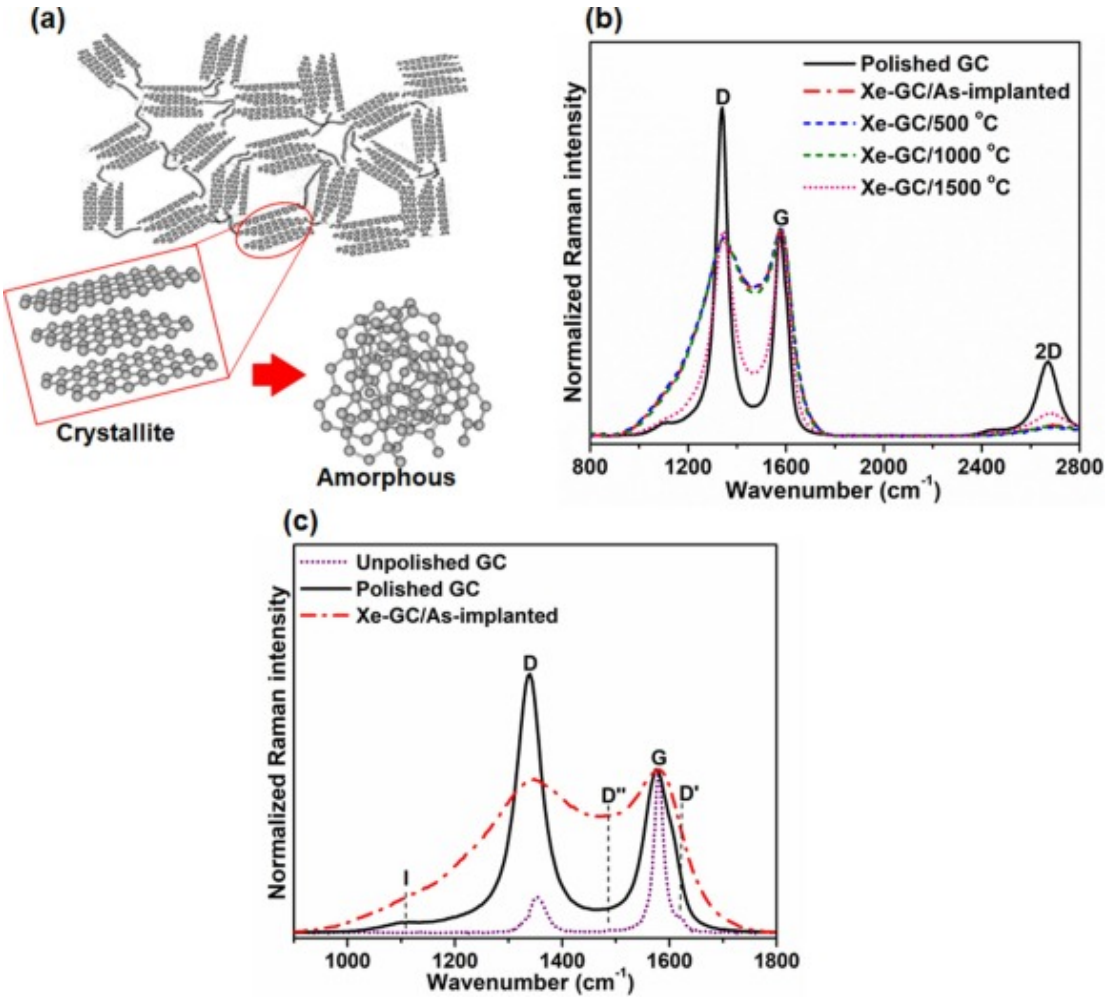

Fig. 2. (a) Schematic illustration of a typical structure of non-graphitizing GC (i.e. Franklin's representation of non-graphitizing carbon). (b) Surface Raman spectra of polished GC, as-implanted Xe-GC, and Xe-GC samples annealed at 500, 1000 and 1500 °C for 5 h. (c) D-to-G bands line-shape of the Raman spectra of unpolished and polished GC, and as-implanted Xe-GC sample.

Moreover, a typical structure of non-graphitizing GC is shown in Fig. 2(a), i.e. Franklin's representation of non-graphitizing carbon [21]. In this model, there are randomly ordered small graphitic crystallites containing few-layer graphene planes, which are joined together by crosslinks and van der Waals force. Also, for an explanation of the low reactivity, hardness, and impermeability of GC, the GC was proposed to have a fullerene-like structure [11]. Furthermore, in the amorphized structure of GC, the graphitic crystallites of GC do not have layered planes, as shown in Fig. 2(a). This transformation of graphitic crystallites into amorphous can be demonstrated by Raman spectroscopy. Fig. 2(b) presents the surface Raman spectra of polished GC, as-implanted Xe-GC, and Xe-GC samples annealed at 500, 1000 and 1500 °C for 5 h. Typically, the Raman characteristic features of carbonaceous materials, GC in this case, are the G-band mode at ~1580 cm^{-1} and the 2D-band mode at ~2670 cm^{-1} which originate from the normal first-order Raman scattering process (the tangential vibration of the sp^2 carbon atoms in graphitic crystallites) and the second-order process (double resonance Raman process) that involves two in-plane transverse optical mode (iTO) phonons near the *K*-point, respectively [22]. An additional band, namely, disorder-induced D-band at ~1350 cm^{-1} is also observed which originates from a double

resonance Raman process involving inter-valley scattering of iTO phonon and defect near the *K*-point [22]. The 2D band is commonly used to determine the number of layers in a few-layer graphene since it only appears from graphitic crystallites containing few-layer graphene planes and is not seen from amorphous carbon (Fig. 2(a)).

In Fig. 2(b), it can be seen that GC shows a 2D band that completely disappears after Xe ion implantation confirming that the graphitic crystallites of GC are amorphized as suggested by SRIM simulations. The Raman spectra of as-implanted Xe-GC, and Xe-GC samples annealed at 500 and 1000 °C are similar suggesting that a series of heat treatments of amorphized GC up to 1000 °C do not recover the initial structure of a non-graphitizing GC. On the contrary, the Raman spectrum of Xe-GC sample annealed up to 1500 °C shows a weak 2D peak intensity and D-to-G bands line-shape almost similar to that of the virgin sample (polished GC) which demonstrates partial structural recovery. A polished GC sample shows high D intensity as compared to the unpolished GC (see Fig. 2(c)) due to surface defects introduced by mechanical polishing of the sample with a diamond solution. However, these surface defects are reduced or transformed into other defects by ion implantation.

To characterise the nature of the surface defects in polished GC, as-implanted and annealed Xe-GC samples, the D-to-G bands line-shape of the Raman spectra were deconvoluted. Fig. 2(c) presents the vibration modes of the D-to-G band line-shape of the Raman spectrum. The origin of D′-band mode at ∼1610 cm^{-1} is related to the carbon lattice vibrations corresponding to that of the G band and is defect activated [23], [24]. The D″-band mode at ∼1490 cm^{-1} originates from the amorphous carbon in the interstitial sites of the carbon lattice, and the origin of the I-band mode at ∼1100 cm^{-1} is related to the lattice vibrations of sp^2-sp^3 bonds and phonon modes in the density of states of graphitic crystallites [24], [25]. To obtain the integrated intensities and the corresponding intensities ratios of the five bands shown in Fig. 2(c), the D-to-G bands line-shape of the Raman spectra of unpolished and polished GC, as-implanted Xe-GC, and Xe-GC samples annealed at 500, 1000 and 1500 °C were fitted with Lorentzian function, as shown in Fig. 3. At high defect concentration, i.e. for polished and as-implanted Xe-GC, the D′ peak merges with the G peak, so to separate the G and D′ peak the positions of the bands were fitted relative to the peak's positions of the original GC (unpolished sample).

Moreover, the G peak shows a dramatic broadening as the D peak broadens upon polishing/implantation (Fig. 4(a)). A broadening of the G peak (from Full width at half maximum (FWHM) of 56.4 to 81.7 cm^{-1}) upon ion implantation can be attributed to a bond-angle disorder, corresponding to the point where the average bond angle changed from the ideal graphitelike 120° as the graphitic crystallites of the implanted GC layer transformed to an amorphous carbon [7]. An increase in the D peak width from 58.4 cm^{-1} to 264.5 cm^{-1} upon ion implantation reflects the introduction of defects into the GC structure which increases bond-angle disorder. At high annealing temperatures above 1000 °C, the D peak of the annealed Xe-GC (at 1500 °C) narrowed from 249.6 to 114.8 cm^{-1} demonstrating structural recovery. The crystallite size, L_a was calculated using the Knight formula [26], [27]:

$$L_a = C(\lambda) / (I_D/I_G) \quad (2)$$

where $C(\lambda)$ is the wavelength-dependent pre-factor estimated as $C(\lambda) \approx C_0 + \lambda C_1$, for $400 < \lambda < 700$ nm. $C(\lambda) = 4.96$ nm for $\lambda = 532$ nm, C_0 and C_1 were estimated to be −12.6 nm and 0.033, respectively, from a plot of $C(\lambda)$ as a function of exciting wavelength [26].

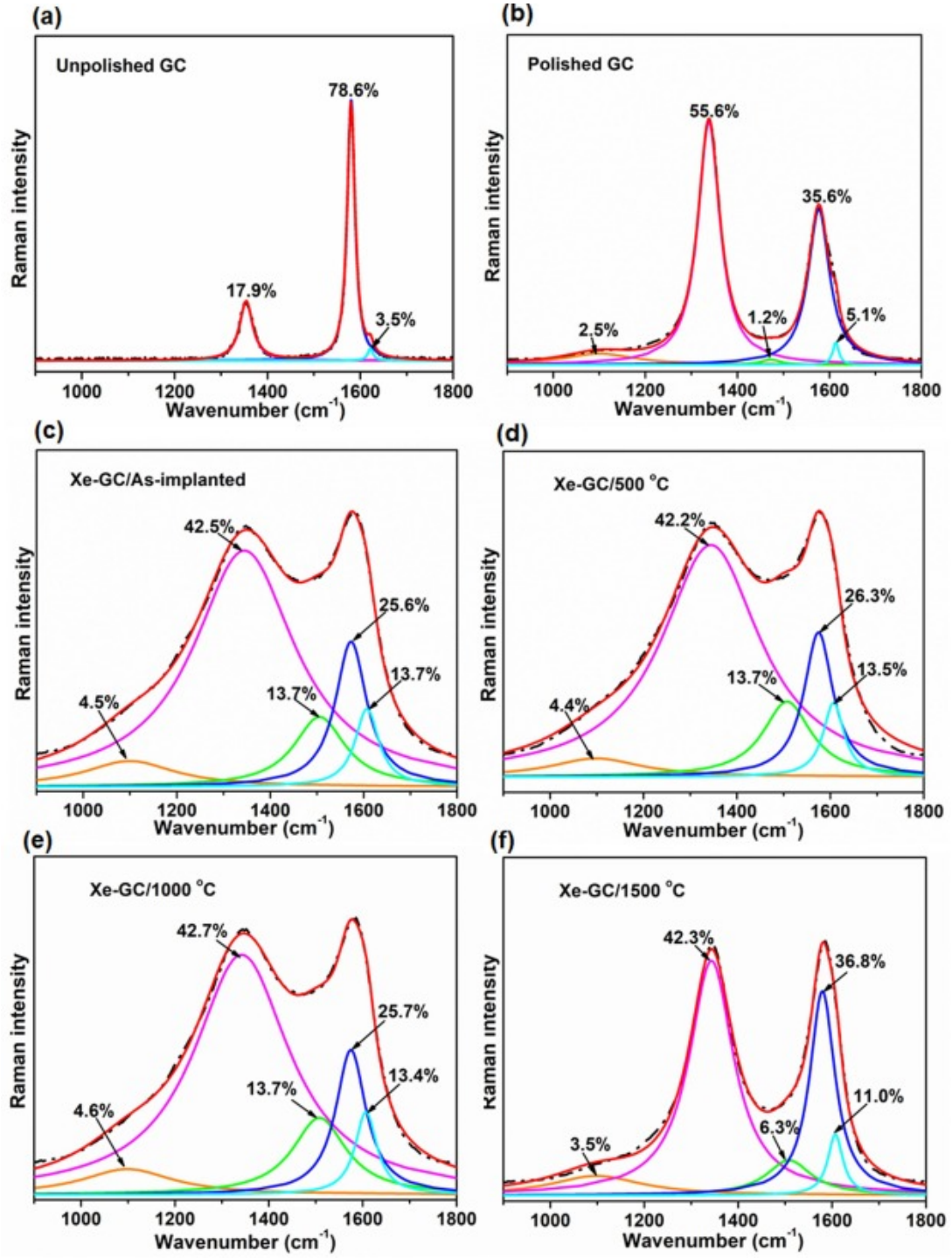

Fig. 3. Raman spectra of (a) unpolished GC, (b) polished GC, (c) as-implanted Xe-GC, and Xe-GC samples annealed at (d) 500, (e) 1000 and (f) 1500 °C for 5 h. The solid lines are the Lorentzian fitting.

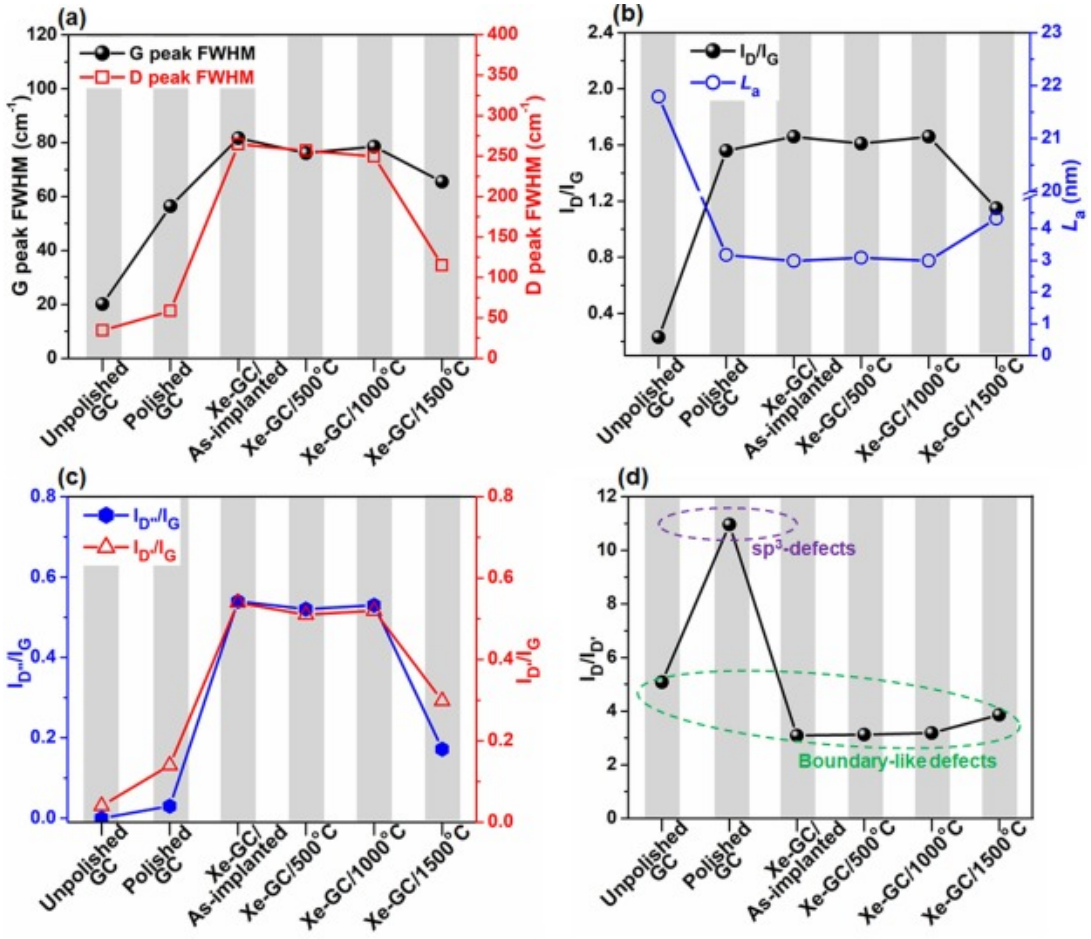

Fig. 4. Raman spectra features: (a) G and D peaks full width at half maximum (FWHM), (b) I_D/I_G ratio and crystallite size (L_a), (c) $I_{D''}/I_G$ and $I_{D'}/I_G$ ratios, and (d) $I_D/I_{D'}$ ratio for unpolished and polished GC, as-implanted Xe-GC, and Xe-GC samples annealed at 500, 1000 and 1500 °C for 5 h.

Fig. 4(b) displays a plot of D-to-G peaks intensities ratio (I_D/I_G) of the Raman spectra of unpolished and polished GC, as-implanted Xe-GC, and Xe-GC samples annealed at 500, 1000 and 1500 °C which shows an initial increase in the I_D/I_G ratio between unpolished and polished GC sample (i.e., from 0.23 for unpolished GC to 1.56 for polished GC). This initial increase in the I_D/I_G ratio due to mechanical polishing of the sample with a diamond solution probably corresponds to a decrease in the in-plane graphitic crystallites size of GC (i.e., from 21.8 nm for unpolished GC to 3.2 nm for polished GC) without amorphization which is introduced by ion implantation. The I_D/I_G ratio of the polished GC is comparable to that of the as-implanted Xe-GC and Xe-GC samples annealed at 500 and 1000 °C. However, for Xe-GC sample annealed at 1500 °C the I_D/I_G ratio decreases from 1.66 to 1.15 which corresponds to an increase in the crystallites size of GC from 3.0 to 4.3 nm.

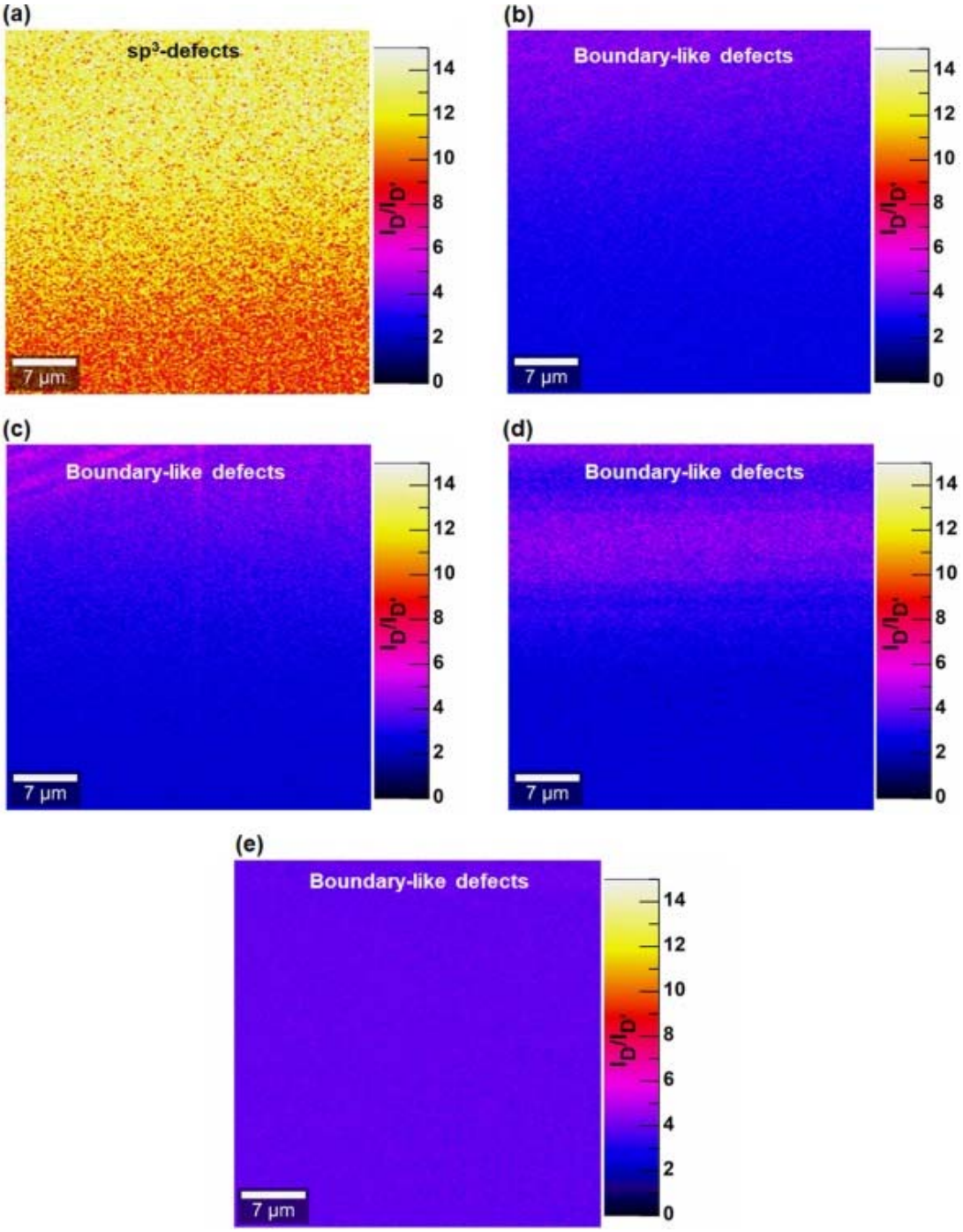

Fig. 5. Raman mapping of $I_D/I_{D'}$ ratio of the integrated intensities of defect-activated modes (D and D′): (a) polished GC, (b) as-implanted Xe-GC, and Xe-GC samples annealed at (c) 500, (d) 1000 and (e) 1500 °C for 5 h.

Fig. 4(c) displays a plot of D″-to-G peaks intensities ratio ($I_{D''}/I_G$), i.e., a ratio of amorphous carbon (D″) relative to the graphitic carbon (G), which shows a dramatic increase in the ratio between polished GC and as-implanted Xe-GC sample (i.e., from 0.03 to 0.54) confirming amorphization of the GC structure upon ion implantation. However, after annealing at temperatures above 1000 °C (at 1500 °C), the $I_{D''}/I_G$ ratio decreases to 0.17 demonstrating

structural recovery. Similarly, a ratio of defect-activated mode (D′) relative to the graphitic carbon (G) ($I_{D'}/I_G$) shows an increase between polished GC and as-implanted Xe-GC sample (i.e., from 0.14 to 0.54), and decreases to 0.30 after annealing at 1500 °C. Moreover, studies have shown that the integrated intensities of defect-activated modes (I_D and $I_{D'}$) are directly proportional to the defect's concentration n_d: $I_D \sim A_d n_d$ and $I_{D'} \sim B_d n_d$, where A_d and B_d are constants which depend on the type of perturbation introduced by the defect in the crystal lattice (i.e., the nature of the defects) [28], [16]. Therefore, $I_D/I_{D'} \sim A_d/B_d$ (i.e., depends only on the type of defects), hence the ratio can be used to get information on the nature of defects [16]. The $I_D/I_{D'} \simeq 13$ for defects associated with sp^3 hybridization, for vacancy-like defects $I_D/I_{D'} \simeq 7$ and $\simeq 3.5$ for boundary-like defects in graphite [16]. These $I_D/I_{D'}$ values for characterising defects were reported by Eckmann et al. [16] using data of ion bombarded graphene, oxidized graphene and graphite with different grain sizes; and are adopted in this study for GC since its structure is made of randomly ordered small graphitic crystallites containing few-layer graphene planes.

Figs. 4(d) and 5 present the nature of surface defects in unpolished and polished GC, as-implanted Xe-GC, and Xe-GC samples annealed at 500, 1000 and 1500 °C. From these results the $I_D/I_{D'}$ ratio is 5.08 (boundary-like defects) for unpolished GC, 11.0 (sp^3-type of defects) for polished GC, 3.1 (boundary-like defects) for as-implanted Xe-GC and Xe-GC samples annealed at 500 and 1000 °C, and 3.8 (boundary-like defects) for a Xe-GC sample annealed at 1500 °C. Therefore, during mechanical polishing of the GC with a diamond solution the in-plane graphitic crystallites size of GC is drastically reduced and the sp^3-type of defects are introduced which describe the out-of-plane atoms bonded to carbon atoms (namely sp^3 hybridization). This type of defects could also originate from the diamond solution molecules which are anchored on GC surface. However, this sp^3-type of defects was modified by ion implantation to boundary-like defects in graphite and did not change during annealing up to 1500 °C.

4. Conclusion

A detailed investigation (SRIM and Raman analyses) of the structural transformation and the nature of surface defects that occurs in GC following mechanical polishing, ion implantation, and annealing have been presented. It was found that ion bombardment with a Xe dose of 1×10^{16} cm^{-2} (6.53 dpa at the surface of the GC) result in GC amorphization which is not recovered by annealing at temperatures ≤1000 °C. However, at a high annealing temperature (1500 °C) about 54% of the amorphized GC structure was recovered as seen from the Raman D peak FWHM which decreased from 249.6 cm^{-1} at 1000 °C to 114.8 cm^{-1} at 1500 °C. It was also found that mechanical polishing of the GC surface before ion implantation drastically reduced the in-plane graphitic crystallites size of GC (from 21.8 to 3.2 nm) and introduced the sp^3-type of defects in the sample. In addition to GC amorphization, ion implantation modified the sp^3-type of defects to boundary-like defects in graphite which did not change during annealing under vacuum conditions. After annealing at a high temperature of 1500 °C, the crystallites size of ion-implanted GC slightly increased from 3.2 to 4.3 nm. A stable disordered/amorphized structure of non-graphitizing ion-implanted GC at high annealing temperatures suggests that GC is a good containment material for Xe. Also, in electrochemistry, such a disordered porous structure of ion-implanted GC would be good since the electrochemical reactions are correlated with a highly disordered porous structure of GC for enhanced performance. It is worth mentioning that at 1500 °C or higher temperatures the structure of the implanted/amorphized GC is transformed into units composed of greater and less-defected graphitelike domains (ordered small graphitic crystallites) resulting in a

decrease in the amount of fullerene-like non-planar sp^2 bond content which is responsible for GC high hardness and strength [2]. So, when the GC is heated at temperatures higher than 1000 °C, it becomes more ordered but weaker. This work demonstrated a detailed analysis of the D-to-G bands line-shape of the Raman spectrum of ion-implanted non-graphitizing GC surface layer (with randomly ordered small graphitic crystallites containing few-layer graphene planes) which can be used to get information on the nature of defects in ion-implanted GC.

CRediT authorship contribution statement

M.J. M.Y.A. Madito Ismail: Conceptualization, Methodology, Investigation, Validation, Writing - original draft, Investigation. **T.T. C.B. Hlatshwayo Mtshali:** Supervision, Funding acquisition, Resources, Supervision, Resources.

Declaration of Competing Interest

The authors declare that they have no known competing financial interests or personal relationships that could have appeared to influence the work reported in this paper.

Acknowledgments

This work is based on the research supported by the National Research Foundation (NRF) of South Africa via iThemba LABS Materials Research Department (MRD) and University of Pretoria (South Africa). Prof. E. Wendler and her team, Institut für Festkörperphysik, Friedrich-Schiller University, Jena, Germany are acknowledged for ion implantation.

References

[1] M.S. Yim, K.L. Murty, Materials issues in nuclear-waste management, *JOM* (2000), https://doi.org/10.1007/s11837-000-0183-0.
[2] K. Jurkiewicz, M. Pawlyta, D. Zygadło, D. Chrobak, S. Duber, R. Wrzalik, A. Ratuszna, A. Burian, Evolution of glassy carbon under heat treatment: Correlation structure–mechanical properties, *J. Mater. Sci.* 53 (2018) 3509–3523, https://doi.org/10.1007/s10853-017-1753-7.
[3] D.F. Langa, N.G. Van Der Berg, E. Friedland, J.B. Malherbe, A.J. Botha, P. Chakraborty, E. Wendler, W. Wesch, Heat treatment of glassy carbon implanted with cesium at room and high temperatures, *Nucl. Instrum. Methods Phys. Res. Sect. B Beam Interact. Mater. Atoms.* 273 (2012) 68–71, https://doi.org/10.1016/j.nimb.2011.07.041.
[4] M.Y.A. Ismail, J.B. Malherbe, O.S. Odutemowo, E.G. Njoroge, T.T. Hlatshwayo, M. Mlambo, E. Wendler, Investigating the effect of heat treatment on the diffusion behaviour of xenon implanted in glassy carbon, *Vacuum* 149 (2018) 74–78, https://doi.org/10.1016/j.vacuum.2017.12.021.
[5] O.S. Odutemowo, J.B. Malherbe, L.C. Prinsloo, E.G. Njoroge, R. Erasmus, E. Wendler, A. Undisz, M. Rettenmayr, Structural and surface changes in glassy carbon due to strontium implantation and heat treatment, *J. Nucl. Mater.* 498 (2018) 103–116, https://doi.org/10.1016/j.jnucmat.2017.10.018.
[6] S. Prawer, F. Ninio, I. Blanchonette, Raman spectroscopic investigation of ion-beam-irradiated glassy carbon, *J. Appl. Phys.* 68 (1990) 2361–2366, https://doi.org/10.1063/1.346547.

[7] D.G. McCulloch, S. Prawer, A. Hoffman, Structural investigation of xenon-ion-beam-irradiated glassy carbon, *Phys. Rev. B.* (1994), https://doi.org/10.1103/PhysRevB.50.5905.
[8] P.J.F. Harris, Fullerene-related structure of commercial glassy carbons, *Philos. Mag.* (2004), https://doi.org/10.1080/14786430410001720363.
[9] P.J.F. Harris, Structure of non-graphitising carbons, *Int. Mater. Rev.* (2014), https://doi.org/10.1179/imr.1997.42.5.206.
[10] P.J.F. Harris, S.C. Tsang, High-resolution electron microscopy studies of non-graphitizing carbons, *Philos. Mag. A Phys. Condens. Matter, Struct. Defects Mech. Prop.* (1997), https://doi.org/10.1080/01418619708214028.
[11] P.J.F. Harris, New perspectives on the structure of graphitic carbons, *Crit. Rev. Solid State Mater. Sci.* (2005), https://doi.org/10.1080/10408430500406265.
[12] M.M. Lucchese, F. Stavale, E.H.M. Ferreira, C. Vilani, M.V.O. Moutinho, R.B. Capaz, C.A. Achete, A. Jorio, Quantifying ion-induced defects and Raman relaxation length in graphene, *Carbon N.Y.* 48 (2010) 1592–1597, https://doi.org/10.1016/j.carbon.2009.12.057.
[13] A. Guermoune, T. Chari, F. Popescu, S.S. Sabri, J. Guillemette, H.S. Skulason, T. Szkopek, M. Siaj, Chemical vapor deposition synthesis of graphene on copper with methanol, ethanol, and propanol precursors, *Carbon N.Y.* 49 (2011) 4204–4210.
[14] E.H.M. Ferreira, Quantifying defects in graphene via Raman spectroscopy at different excitation energies, *Nano Letters* 11 (2011) 3190–3196, https://doi.org/10.1021/nl201432g.
[15] A.C. Ferrari, D.M. Basko, Raman spectroscopy as a versatile tool for studying the properties of graphene, *Nat. Nanotechnol*. 8 (2013) 235–246, https://doi.org/10.1038/nnano.2013.46.
[16] A. Eckmann, A. Felten, A. Mishchenko, L. Britnell, R. Krupke, K.S. Novoselov, C. Casiraghi, Probing the nature of defects in graphene by Raman spectroscopy, *Nano Letters* 12 (2012) 3925–3930, https://doi.org/10.1021/nl300901a.
[17] O.S. Odutemowo, J.B. Malherbe, L. Prinsloo, D.F. Langa, E. Wendler, High temperature annealing studies of strontium ion implanted glassy carbon, *Nucl. Instrum. Methods Phys. Res. Sect. B Beam Interact. Mater. Atoms.* (2016), https://doi.org/10.1016/j.nimb.2015.10.054.
[18] J.B. Malherbe, O.S. Odutemowo, E.G. Njoroge, D.F. Langa, T.T. Hlatshwayo, C.C. Theron, Ion bombardment of glassy carbon, *Vacuum (*2018), https://doi.org/10.1016/j.vacuum.2017.11.006.
[19] A.J. Mckenna, T. Trevethan, C.D. Latham, P.J. Young, M.I. Heggie, Threshold displacement energy and damage function in graphite from molecular dynamics, *Carbon N.Y.* 99 (2016) 71–78, https://doi.org/10.1016/j.carbon.2015.11.040.
[20] R.E. Stoller, M.B. Toloczko, G.S. Was, A.G. Certain, S. Dwaraknath, F.A. Garner, On the use of SRIM for computing radiation damage exposure, *Nucl. Instrum. Methods Phys. Res. Sect. B Beam Interact. Mater. Atoms.* 310 (2013) 75–80, https://doi.org/10.1016/J.NIMB.2013.05.008.
[21] R.E. Franklin, Crystallite growth in graphitizing and non-graphitizing carbons, *Proc. R. Soc. London. Ser. A. Math. Phys. Sci.* 209 (1951) 196–218, https://doi.org/10.1098/rspa.1951.0197.
[22] A.C. Ferrari, J.C. Meyer, V. Scardaci, C. Casiraghi, M. Lazzeri, F. Mauri, S. Piscanec, D. Jiang, K.S. Novoselov, S. Roth, A.K. Geim, Raman spectrum of graphene and graphene layers, *Phys. Rev. Lett.* 97 (2006) 187401.
[23] Y. Wang, D.C. Alsmeyer, R.L. McCreery, Raman spectroscopy of carbon materials: structural basis of observed spectra, *Chem. Mater.* 2 (1990) 557–563, https://doi.org/10.1021/cm00011a018.
[24] A. Sadezky, H. Muckenhuber, H. Grothe, R. Niessner, U. Poschl, Raman micro-spectroscopy of soot and related carbonaceous materials: Spectral analysis and structural

information, *Carbon N.Y.* 43 (2005) 1731–1742, https://doi.org/10.1016/j.carbon.2005.02.018.
[25] A.C. Ferrari, J. Robertson, Interpretation of Raman spectra of disordered and amorphous carbon, *Phys. Rev. B.* 61 (2000) 14095–14107, https://doi.org/10.1103/PhysRevB.61.14095.
[26] M. Endo, M.A. Pimenta, Origin of dispersive effects of the Raman d band in carbon materials, *Phys. Rev. B - Condens. Matter Mater. Phys.* 59 (1999) R6585–R6588, https://doi.org/10.1103/PhysRevB.59.R6585.
[27] H. Zhang, L. Zhang, J. Chen, H. Su, F. Liu, W. Yang, One-step synthesis of hierarchically porous carbons for high-performance electric double layer supercapacitors, J. *Power Sources* 315 (2016) 120–126, https://doi.org/10.1613/jair.301.
[28] P. Venezuela, M. Lazzeri, F. Mauri, Theory of double-resonant Raman spectra in graphene: Intensity and line shape of defect-induced and two-phonon bands, *Phys. Rev. B - Condens. Matter Mater. Phys.* 84 (2011), https://doi.org/10.1103/PhysRevB.84.035433